Microporous and Mesoporous Materials 220 (2016) 258–269

Contents lists available at ScienceDirect

Microporous and Mesoporous Materials

journal homepage: www.elsevier.com/locate/micromeso

Prospects of monolithic MIL-MOF@poly(NIPAM)HIPE composites as water sorption materials

Martin Wickenheisser, Tanja Paul, Christoph Janiak*

Institut für Anorganische Chemie und Strukturchemie I, Universitätsstraße 1, 40225 Düsseldorf, Germany

ARTICLE INFO

Article history:
Received 7 July 2015
Received in revised form
20 August 2015
Accepted 5 September 2015
Available online 12 September 2015

Keywords:
Functional composites
Hybrid composites
Metal-organic framework
High internal phase emulsions (HIPE)
Water adsorption

ABSTRACT

Monolithic shaping of metal-organic frameworks (MOFs), which are normally received as microcrystalline powder is crucial for possible applications of MOFs. Three members of the MIL-family (MIL-100(Fe), MIL-100(Cr) and MIL-101(Cr)), known as water stable porous coordination polymers, were embedded into a macroporous oil–water (o/w) high internal phase emulsion (HIPE) foam, based on cross-linked poly(*N*-isopropyl acrylamide) (NIPAM). Pre-polymerization of the HIPE emulsions before adding the MIL-MOF powders was an indispensable step in synthesizing highly porous composites, thus, minimizing pore blocking effects. The larger the pores and the higher the surface area of the MIL the less pronounced were pore blocking effects upon composite formation. These composite materials (MIL@-poly(NIPAM)HIPE, in short MIL@NIPAM) could be loaded with up to 92 wt% of the MIL component (followed and verified by powder X-ray diffractometry, infrared spectroscopy and scanning electron microscopy). MIL@NIPAM composites show higher water vapor uptakes in comparison to the native HIPE material so that MIL@NIPAM composites could be used as monolithic water sorbents for heat transformation applications. For MIL-101(Cr)@NIPAM the water uptake of up to 0.4 g/g occurs with the typical S-shaped isotherm in the range of $0.3 < P \cdot P_0^{-1} < 0.5$.

1. Introduction

Metal-organic frameworks (MOFs) are three-dimensional coordination networks, built from metal ions or metal clusters (nodes), connected by multidentate organic ligands, with potential porosity [1]. The crystalline MOFs have uniform micro-/mesoporous structures with high surface areas and exhibit guest exchange properties which is the basis for possible applications [2–4] such as catalysis [5–9] gas storage [10–13], gas separation [14–18]. Various review articles are evidence to the steady interest in MOFs [19–26].

Recently MOFs are investigated in connection with sorption-based environmentally friendly heating and cooling technologies [24–30]. Electrical energy consumption by conventional air-conditioners accounts for 30–50% of the total electric energy consumed in modern buildings during hot seasons [31]. Sorption-based heat transformations require about one third electrical power of a conventional compressor air-conditioner and make use of low temperature waste heat or solar thermal heat as driving energy [28,30]. Thus, thermally driven adsorption chillers (TDC) or adsorption heat pumps (AHP) represent promising alternatives for traditional cooling or heating devices in terms of saving electrical energy and thereby reducing greenhouse gas emission for electricity production.

The basic principle of a vapor sorption based chiller or heat pump is illustrated in Fig. 1. It consists of a vessel containing the dehydrated (activated), porous adsorbent (e.g. a zeolite, silica gel or a MOF) and another vessel, which includes the working fluid (e.g. water). Water is a desired working fluid as it is non-toxic and has a high evaporation enthalpy (2440 kJ mol^{-1} at 25 °C) [24–26]. During the production cycle, the working fluid is evaporated, which generates useful cold in a cooling case and the heat of adsorption is released to the environment, or used when the device is operated as a heat pump. For regeneration of the porous adsorbent, heat from an external source such as a solar collector or waste heat is applied to desorb the working fluid, which is condensed to release heat of condensation. In the heat pump mode, this heat is used. In a cooling application it is rejected to the environment. Water vapor is exchanged reversibly within the production/regeneration cycle.

* Corresponding author.
E-mail address: janiak@uni-duesseldorf.de (C. Janiak).

http://dx.doi.org/10.1016/j.micromeso.2015.09.008
1387-1811/

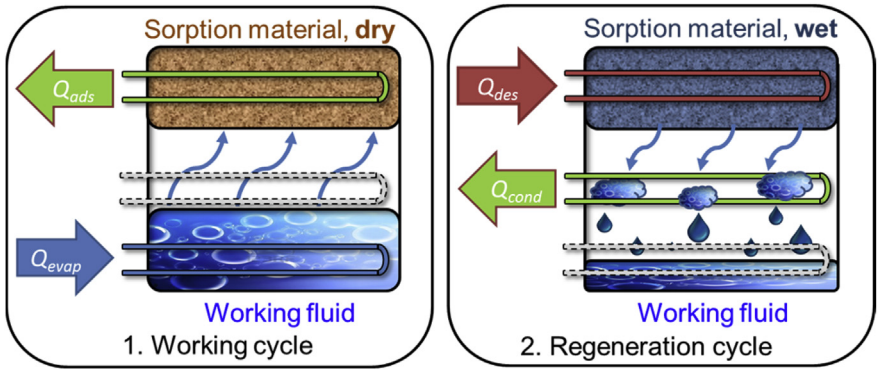

Fig. 1. Principle of thermally driven adsorption chillers (TDC) or adsorption heat pumps (AHP). Left – working cycle: Water or another working fluid is vaporized at a low pressure, by drawing heat of evaporation Q_{evap} from the environment. Water vapor is adsorbed to the (dry) sorption material, giving off heat of adsorption Q_{ads}. Right – regeneration cycle: The loaded sorption material is dried again by applying driving heat Q_{des} for desorption. The working fluid desorbs and is condensed at a medium temperature level releasing heat of condensation Q_{cond}.

Micro/mesoporous MIL-101(Cr), $\{Cr_3(\mu_3\text{-}O)(F,OH)(H_2O)_2(BDC)_3\cdot\sim 25H_2O\}_n$ (BDC = benzene-1,4-dicarboxylate, terephthalate) is a chromium(III)-terephthalate MOF with BET surface areas up to 4100 $m^2\ g^{-1}$ [32] and was shown to be a promising candidate for heat transformation applications due to its S-shaped water adsorption isotherm with loading lifts of 1.0–1.5 g g^{-1} [33]. MIL-101 features a zeotype structure with cages of 29 Å and 34 Å in diameter (Fig. 2) [32]. Water cycling tests have only shown a slight degradation of approximately 3% after 40 ad-/desorption cycles [33].

Metal-organic frameworks of the MIL-100 type (MIL = Materials of Institute Lavoisier), namely $\{M_3(\mu_3\text{-}O)(OH,F)(H_2O)_2(BTC)_2\cdot\sim nH_2O\}$ (M = Cr^{3+} [35], Fe^{3+} [36], Al^{3+} [37], BTC = benzene-1,3,5-tricarboxylate, trimesate) are further potential adsorbents for AHP and TDC applications. Again, two types of mesoporous cages of 25 Å and 29 Å in diameter form the zeotype structure, with surface areas of 1500–2000 $m^2\ g^{-1}$ (Fig. 3). The desired S-shaped adsorption isotherms showed water loading lifts of 0.6–0.7 g g^{-1} for MIL-100(Cr), 0.65–0.75 g g^{-1} for MIL-

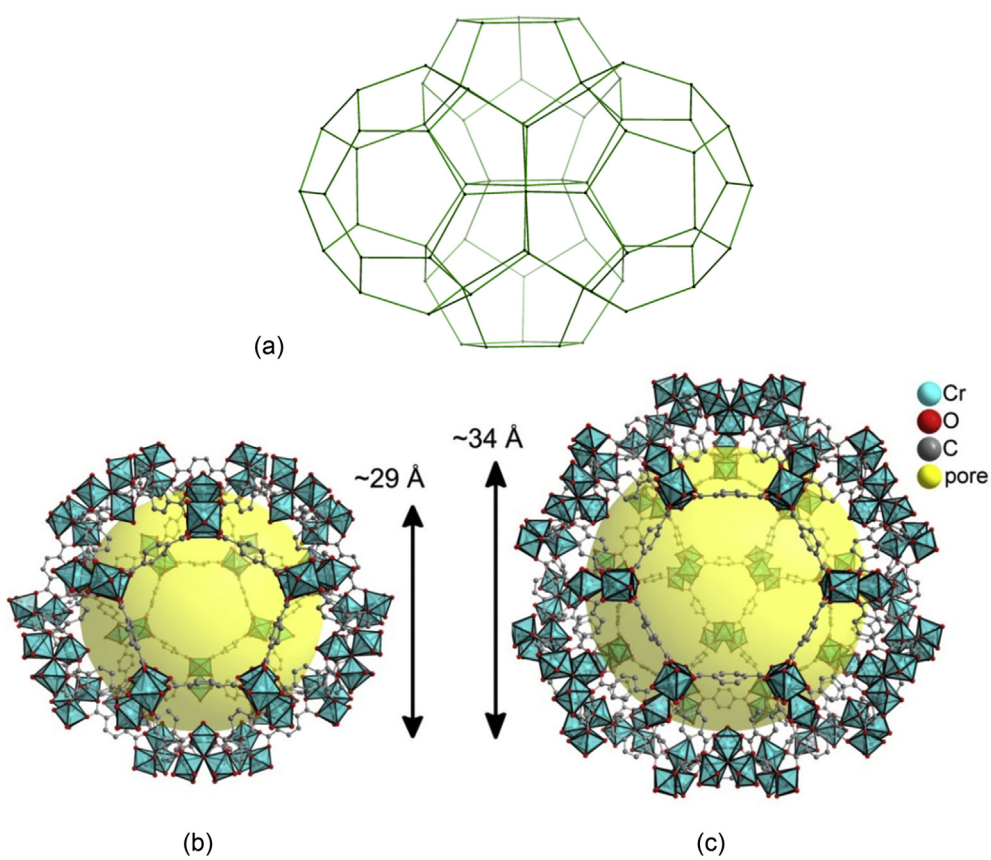

Fig. 2. MIL-101(Cr): (a) mesoporous network; (b) small cage with pentagonal windows; (c) large cage with pentagonal and hexagonal windows; Objects are not drawn to scale. The yellow spheres in the mesoporous cages with the indicated diameters take into account the van-der-Waals radii of the framework walls. Hydrogen atoms and solvent molecules of crystallization are not shown. Graphics have been drawn with DIAMOND [34] from the deposited cif-file for MIL-101(Cr) (CSD-Refcode OCUNAK) [32]. (For interpretation of the references to colour in this figure legend, the reader is referred to the web version of this article.)

100(Fe) and 0.5 g g^{-1} for MIL-100(Al) and promising cycling stabilities [38,39].

Bulk metal-organic frameworks, are synthesized as fine (micro-)crystalline powders. For large-scale handling and in realistic applications MOFs require appropriate shaping with binders [40] or by pressing into tables or pellets [41] to avoid, e.g., dust formation. It is a challenge to shape MOFs without losing their porosity and simultaneously achieve mechanically stable bodies [42]. This is a rapidly growing research, which has been recently reviewed by Bradshaw and co-workers and Xu et al. [43,44].

High internal phase emulsion (HIPE) polymerization is a synthetic technique to obtain monolithic, macroporous polymers [45]. In a conventional emulsion the internal/dispersed phase is insoluble in the continuous phase. When the volume fraction of the dispersed phase is increased to 74%, which is the maximum packing fraction for equal spheres, the dispersed phase is surrounded by a thin film of the external/continuous phase. This specific state is named 'HIPE' [46]. After polymerization of the monomers and cross-linkers in the continuous phase and removal of the internal phase by washing steps, a monolithic macroporous polyHIPE material of low density (<0.1 g cm^{-3}) can be obtained. PolyHIPEs possess a special open cell structure with two kinds of macropores. The larger voids of approximately 0.5–600 μm in diameter, induced by the droplets of the internal phase, are connected by the smaller windows of approximately 0.1–300 μm in diameter [46]. Due to their macroporous nature, polyHIPEs show BET surface areas of less than 50 m^2 g^{-1}.

(Meth-)acrylic monomers as well as other vinyl monomers such as acrylonitrile [47] and *N*-isopropyl acrylamide [48] have been utilized to synthesize monolithic polyHIPE bodies. The monomers, used in water/oil (w/o) HIPE systems, are hydrophobic and the polymerization of the continuous, oily phase also leads to hydrophobic products. Intended hydrophilic polyHIPEs are obtained by polymerization of hydrophilic monomers in the aqueous phase of oil/water (o/w) HIPEs. Control over HIPE structures can be obtained by fine-tuning parameters such as the ratio of both phases, choice of monomers and surfactants, degree of cross-linking, temperature, curing time and several others [49–52].

In this work, we report the embedding of water stable MIL-100(Fe and Cr) and MIL-101(Cr) particles in supposedly hydrophilic poly(NIPAM)HIPE (NIPAM = *N*-isopropyl acrylamide) for water sorption application.

2. Experimental section

2.1. Materials and methods

All chemicals were obtained commercially and were used without further purification. Iron powder (Riedel-de Haën, >99%), CrO_3 (Alfa Aesar, 99%), $Cr(NO_3)_3 \cdot 9H_2O$ (Acros Organics, 99%), hydrofluoric acid (Acros Organics, 48–51 wt% in H_2O), HNO_3 (Grüssing, 65 wt%), 1,3,5-benzenetricarboxylic acid (H_3BTC) (Alfa Aesar, 98%), benzene-1,4-dicarboxylic acid (H_2BDC) (Acros Organics, >99%), tetramethylammonium hydroxide (TMAOH) (Alfa Aesar, 25 wt% in water), *N*-isopropyl acrylamide (NIPAM) (TCI, stabilized with 4-methoxyphenol), *N*,*N*′-methylenebisacrylamide (MBA) (Sigma–Aldrich, 99%), Triton™-X-405 (Sigma–Aldrich, 70% in H_2O), ammonium persulfate (APS) (ROTH, ≥98%), *N*,*N*,*N*′,*N*′-tetramethylethylenediamine (TMEDA) (Merck KGaA, >99%), *N*,*N*'-dimethylformamide (DMF) (VWR, p.a.), ethanol (VWR, p.a.), cyclohexane (Applichem, p.a.). All experimental work was performed in air.

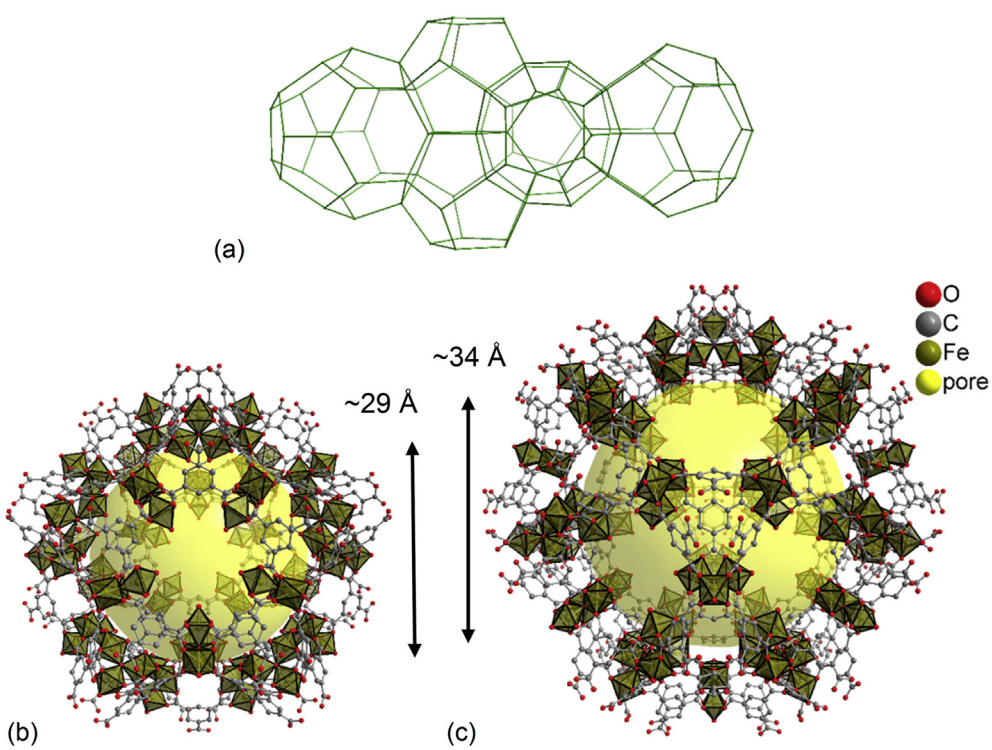

Fig. 3. MIL-100(*M*): (a) mesoporous network; (b) small cage with pentagonal windows; (c) large cage with pentagonal and hexagonal windows; Objects are not drawn to scale. The yellow spheres in the mesoporous cages with the indicated diameters take into account the van-der-Waals radii of the framework walls. Hydrogen atoms and solvent molecules of crystallization are not shown. Graphics have been drawn with DIAMOND [34] from the deposited cif-file for CCDC number 648835, Refcode UDEMEW for Cr [35], CCDC 640536, CIGXIA for Fe [36]. (For interpretation of the references to colour in this figure legend, the reader is referred to the web version of this article.)

2.2. Physical measurements

Powder X-ray diffraction (PXRD) was carried out at ambient temperature on a Bruker D2 Phaser with a flat sample holder using Cu-Kα radiation (λ = 1.54182 Å). Fourier transform infrared spectra were obtained on a Bruker TENSOR 37 IR spectrometer at ambient temperature as KBr disks in the range of 4000–500 cm^{-1}. Nitrogen physisorption isotherms were measured on a Nova 4000e from Quantachrome at 77 K. BET surface areas were calculated from the nitrogen physisorption isotherms. DFT calculations for the pore size distribution curves were done with the native NovaWin 11.03 software using the 'N_2 at 77 K on carbon, slit pore, nonlinear density functional theory (NLDFT) equilibrium' model [53–55]. Water physisorption isotherms were measured volumetrically on a Quantachrome Autosorb iQ MP at 293 K. For measuring the isotherms the materials were loaded into glass tubes capped with septa. The weighed tubes were attached to the corresponding degassing port of the sorption analyzer, degassed under vacuum at elevated temperature, weighed again and then transferred to the analysis port of the sorption analyzer. Scanning electron microscopic (SEM) images were collected on a LEO 1430 VP from Zeiss. The samples were coated with Au for 180 s at 30 mA by an AGAR sputter.

2.3. Synthesis of MIL-100(Fe,Cr) and MIL-101(Cr)

MIL-100(Fe), MIL-100(Cr) and MIL-101(Cr) were hydrothermally synthesized according to the literature [56–58]. Typical batch sizes of 665 mg iron powder (11.9 mmol), 1.65 g H_3BTC (7.85 mmol), 0.83 mL hydrofluoric acid (24 mmol; 48–51 wt% in H_2O), 0.5 mL HNO_3 (7 mmol; 65 wt%) and 60 mL of deionized H_2O (for MIL-100(Fe)), 1.20 g CrO_3 (12.0 mmol), 2.52 g H_3BTC (12.0 mmol), 0.42 mL hydrofluoric acid (12 mmol; 48–51 wt% in H_2O) and 58 mL of deionized H_2O (for MIL-100(Cr)) and 4.80 g (12.0 mmol) $Cr(NO_3)_3 \cdot 9H_2O$, 1.98 g (11.9 mmol) H_2BDC, 1.1 mL TMAOH (3.1 mmol; $\rho = 1.014$ g mL^{-1}; 25 wt% in H_2O) and 60 mL of deionized water (for MIL-101(Cr)) yielded the as-synthesized MILs. For activation the MILs were purified through a consecutive washing procedure with DMF, EtOH and deionized water (see Supplementary data for details). Amounts of 1.50, 3.18 and 2.34 g of purified MIL-100(Fe), MIL-100(Cr) and MIL-101(Cr), respectively, were isolated (41, 69 and 50% yield based on Fe or Cr), as orange-brown MIL-100(Fe) and green MIL-100/101(Cr) powders with BET surface areas and pore volumes shown in Table 1. Pore volumes (measured at $P \cdot P_0^{-1} = 0.95$) and BET surface areas were calculated from the type I N_2 sorption isotherms (Fig. A.2a, A.4a, A.6a, Table 1). BET surface areas of the MOF starting materials (2140 m^2 g^{-1} MIL-100(Fe); 1370 m^2 g^{-1} MIL-100(Cr); 2860 m^2 g^{-1} MIL-101(Cr), Table 1) were in agreement with literature values (see ranges and references given in Table 1, footnote f, g, h). Experimental, theoretical powder X-ray patterns and the IR-spectra are shown in Fig. A.1, A.3, A.5.

2.4. Synthesis of native poly(NIPAM)HIPE

Poly(NIPAM)HIPEs with 9, 13 and 17 mol% of *N*,*N*′-methylenebisacrylamide were prepared according to the literature [59]. In brief: Aqueous solutions of 4.0 mL each of *N*-isopropyl acrylamide (NIPAM, 1.0 mol L^{-1}, 4.0 mmol) and *N*,*N*′-methylenebisacrylamide (MBA, 0.05 mol L^{-1}, 0.2 mmol) were added into 50 mL beakers. Different amounts of additional solid MBA (30 mg, 62 mg or 92 mg MBA, respectively) were then added to the solutions under constant stirring. The surfactant Triton™-X-405 was added followed by aqueous ammonium persulfate solution as the radical initiator. After stirring for 10 min, the oily phase cyclohexane was slowly dropped into each solution continued by further stirring for 10 min. *N*,*N*,*N*′,*N*′-tetramethylethylenediamine (TMEDA) which acts together with APS as radical initiator was added followed by stirring for 10 min. The white, viscous dispersions were filled into Teflon-liners and cured for 3 days at 333 K. A washing procedure with deionized water for each product was followed by air-drying of the monoliths. White materials were isolated which are differentiated by the relative total content of 9, 13 and 17 mol% MBA. Poly(NIPAM)HIPE with 17 mol% of total MBA led to a monolithic body even though shrinkage of approximately 50% of the original volume occurred during drying. Using 9 and 13 mol% of cross-linking led to monoliths with pronounced shrinkage, deformation and cracks.

3. Results and discussion

3.1. Native poly(NIPAM)HIPE

The synthesis of poly(NIPAM)HIPEs according to the literature [59] consists of cross-linking *N*-isopropyl acrylamide with *N*,*N*′-methylenebisacrylamide in a radical polymerization (Scheme 1). To the best of our knowledge poly(NIPAM)HIPEs with MBA cross-linking of only 1–5 mol% have been reported so far. Based on our experimental experience and other literature, these reported monoliths shrank considerably during drying, accompanied by large cracks [59]. Increasing the degree of cross-linking should enhance the mechanical stability for the derived monoliths, yielding a more rigid and resistant material towards shrinkage [46,60,61].

Therefore, additional amounts of MBA to bring the total to 9, 13 or 17 mol%, respectively, were added to increase the degree of cross-linking. Still, only poly(NIPAM)HIPE with 17 mol% of MBA yielded a monolithic body although shrinkage of approximately 50% of the original volume was observed during drying (Fig. 4a). With 9 and 13 mol% of MBA the monoliths still exhibited large shrinkage, deformation and cracks upon drying. This shrinkage is in agreement with poly(NIPAM)HIPEs reported in the literature [59].

Scanning electron microscopic images of poly(NIPAM)HIPEs with 9, 13 and 17 mol% of MBA are displayed in Fig. 4b,c,d. The average void sizes for all three materials are in the range of 20–110 μm. Literature-known poly(NIPAM)HIPEs with 1 and 2 mol % MBA show a bimodal pore size distribution with voids of 1–2 μm and 60 μm (Fig. 5b). A cross-linking amount of 5 mol% of MBA led to void diameters of 10 μm [59]. A strict correlation between degree of cross-linking and void size seems not to be apparent.

Infrared spectra of poly(NIPAM)HIPEs are shown in Fig. A.9 and are consistent with other literature data [62]. A typical water sorption isotherm of native poly(NIPAM)HIPE (17 mol% MBA) is shown in Fig. 5.

A low BET surface area of 20 m^2 g^{-1} is typical for HIPE systems due to their macroporous character. Macropores are by IUPAC definition larger than 50 nm [63]. It has to be mentioned that porosity of such macroporous systems should better be evaluated from mercury intrusion porosimetry experiments, which is the appropriate method for the analysis of pores between 3 nm and 950 μm. Porosity analysis based on gas physisorption is limited to pore sizes with diameters of 400 nm and below. The pore size distribution curve of poly(NIPAM)HIPE (1% MBA cross-linking), calculated from mercury intrusion measurements, was taken from the literature and displayed in Fig. 5b. The pore sizes of approximately 60.4 (±0.1) μm and 1.6 (±0.1) μm, found by mercury porosimetry reflect the size of the voids and the connecting pores [59].

The water vapor sorption isotherm of native poly(NIPAM)HIPE (17 mol% MBA) shows a rather hydrophobic shape based on its parabolic shape (type III) (Fig. 5a) according to the IUPAC

Table 1
Results from nitrogen and water sorption measurements.[a]

Sample[a]	Porosity data			Water adsorption values[e]		
	S(BET) meas.[b] ($m^2\ g^{-1}$)	*S*(BET) calc.[c] ($m^2\ g^{-1}$)	*V*(pore), ($cm^3\ g^{-1}$)[d]	Meas.[e] ($g\ g^{-1}$)	Calc.[f] ($g\ g^{-1}$)	Rel. To surface area[g] ($\times 10^{-3}\ g\ m^{-2}$)
Native poly(NIPAM) HIPE (17 mol% MBA)	20	–	0.03	0.26	–	13
Bulk MIL-100(Fe)	2140	–	0.88	0.65–0.75[h]	–	0.33
MIL-100(Fe)-NIPAM composites:						
37 wt% MIL-100(Fe)	230	800	0.12	0.25	0.42	1.09
78 wt% MIL-100(Fe)	300	1650	0.16	0.27	0.60	0.90
Bulk MIL-100(Cr)	1370	–	0.84	0.6–0.7[h]	–	0.47
MIL-100(Cr)-NIPAM composites:						
49 wt% MIL-100(Cr)	90	680	0.14	0.25	0.45	2.78
58 wt% MIL-100(Cr)	150	800	0.17	0.26	0.49	1.73
Bulk MIL-101(Cr)	2860	–	1.35	1.0–1.5[h]	–	0.44
MIL-101(Cr)-NIPAM composites:						
46 wt% MIL-101(Cr)	720	1320	0.37	0.36	0.72	0.50
71 wt% MIL-101(Cr)	960	2030	0.47	0.42	0.96	0.44
92 wt% MIL-101(Cr)	980	2630	0.50	n.d.[i]		

[a] Wt% refers to MIL amount in the composites. Quantification of the MIL content by weight percent, assumes that no MOF was lost during the synthesis: wt% (MIL in MIL@NIPAM) = (m (weighted MIL)/m (MIL@NIPAM)) × 100.
[b] *S*(BET) measured from N_2 sorption isotherm 77 K with a standard deviation ± 20 $m^2\ g^{-1}$ (calculated at $0.05 < P \cdot P_0^{-1} < 0.2$).
[c] *S*(BET) calculated (estimated) as the sum of the mass-weighted surface areas of the MILs (MIL-100(Fe) = 2140 $m^2\ g^{-1}$; MIL-100(Cr) = 1370 $m^2\ g^{-1}$; MIL-101(Cr) = 2860 $m^2\ g^{-1}$) and pure poly(NIPAM)HIPE (20 $m^2\ g^{-1}$) from following formula: BET calc = (wt% of HIPE/100) × 20 $m^2\ g^{-1}$ + (wt% of MIL/100)× 2140 (MIL – 100Fe) or 1370 (MIL – 100Cr) or 2860 (MIL – 101Cr) $m^2\ g^{-1}$.
[d] Total pore volume V(pore) calculated from N_2 sorption isotherm at 77 K ($P\ P_0^{-1} = 0.95$) for pores ≤ 20 nm.
[e] Water adsorption value measured from water sorption isotherm at 293 K ($P\ P_0^{-1} = 0.9$).
[f] Water adsorption value calculated (estimated) as the sum of the mass-weighted uptakes at $P \cdot P_0^{-1} = 0.9$ of the MILs (MIL-100(Fe) = 0.70 $g\ g^{-1}$; MIL-100(Cr) = 0.65 $g\ g^{-1}$; MIL-101(Cr) = 1.25 $g\ g^{-1}$) and poly(NIPAM)HIPE (0.26 $g\ g^{-1}$) from following formula: Water adsorption calc = (wt% of HIPE/100) × 0.26 $g\ g^{-1}$+ (wt% of MIL/100) × 0.70 (MIL – 100Fe) or 0.65 (MIL – 100Cr) or 1.25 (MIL – 101Cr) $g\ g^{-1}$.
[g] Water adsorption value calculated relative to the measured BET surface area of the MIL or MIL@NIPAM composite according to following formula: Water adsorption calculated relative to surface area = (water adsorption measured in $g\ g^{-1}$/S(BET) measured in $m^2\ g^{-1}$)[$g\ m^{-2}$] for example: for MIL-100(Fe): 0.70 $g\ g^{-1}$/ 2140 $m^2\ g^{-1}$ = 0.00033 $g\ m^{-2}$ = 0.33 × 10^{-3} $g\ m^{-2}$.
[h] Range of water uptake capacities based on our experimental data.
[i] n.d. = not determined.

classification [64]. When poly(NIPAM)HIPEs are classified as "hydrophilic" in the literature this is based on the immersion of the material in water for a specified time to then determine the gravimetric water uptake, e.g., to 8000% w/w [65]. Here we have to use water *vapor* adsorption in line with the intended application for adsorption chillers (TDC) or adsorption heat pumps (AHP). It is noteworthy that poly(NIPAM)HIPEs can no longer be considered hydrophilic when it comes to water *vapor* sorption. Instead they are rather hydrophobic despite the total water uptake of 0.26 $g\ g^{-1}$ at $P \cdot P_0^{-1} = 0.9$ (Table 1). The water uptake of 0.26 $g\ g^{-1}$ is reached close to the saturation pressure of $P \cdot P_0^{-1} = 0.9$ (Fig. 8c) and such a water uptake is also seen for water vapor sorption of active carbons (0.3 $g\ g^{-1}$) [66]. Yet, for the small poly(NIPAM)HIPE surface area of 20 $m^2\ g^{-1}$ such a water uptake of 0.26 $g\ g^{-1}$ can be considered high and is due to pore condensation near the saturation pressure.

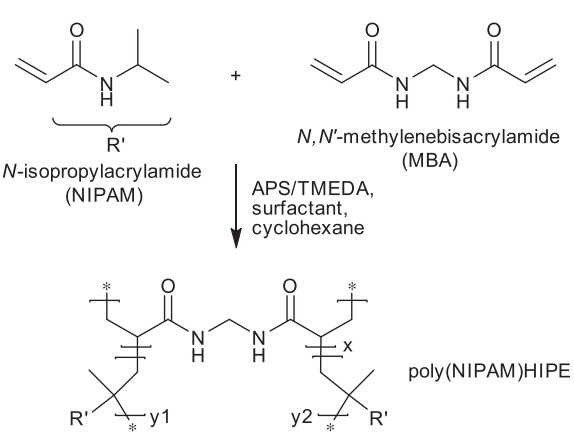

Scheme 1. Radical polymerization of *N*-isopropyl acrylamide (NIPAM) and *N,N'*-methylenebisacrylamide (MBA) initiated by ammonium persulfate (APS) (x = 9, 13 or 17 mol%, y1 + y2 = 91, 87 or 73 mol%, respectively).

3.2. Embedding MIL-100(Fe,Cr) and MIL-101(Cr) into poly(NIPAM) HIPE

Different samples of MIL@poly(NIPAM)HIPEs (in short MIL@-NIPAM) were synthesized by simply adding pre-formed MIL powders to the poly(NIPAM)HIPE emulsion. Pre-polymerization of the HIPE emulsion before adding MOF powders was found to be an indispensable factor for highly porous MIL@HIPE composites (see Supp. Info.). Without pre-polymerization pore blocking of the MOF by monomer inclusion from the HIPE emulsion occurs [40,42].

The syntheses of MIL@NIPAM composites containing different weight percentages of MIL, were done by a modified procedure of pure poly(NIPAM)HIPE. Various amounts of well-ground MIL-100(Fe), MIL-100(Cr) and MIL-101(Cr) powders were filled into 5 mL plastic syringes followed by adding specific amounts of pre-polymerized NIPAM-HIPE emulsion (with 17 mol% MBA). After homogenization, curing, washing and drying orange-brown MIL-100(Fe)@NIPAM (37 and 78 wt% MIL), green (ii) MIL-100(Cr) @NIPAM (49, 58 wt% MIL) and green MIL-101(Cr)@NIPAM (46, 71, 92 wt% MIL) materials were obtained (see Supp. Info.). Still, all these composites shrank during drying similar to native poly(-NIPAM)HIPE (Figs. 6a and 11a). The composites were prepared in a cylinder-shaped syringe container. Upon drying, however, the composite bodies shrank considerably and formed unsymmetrical

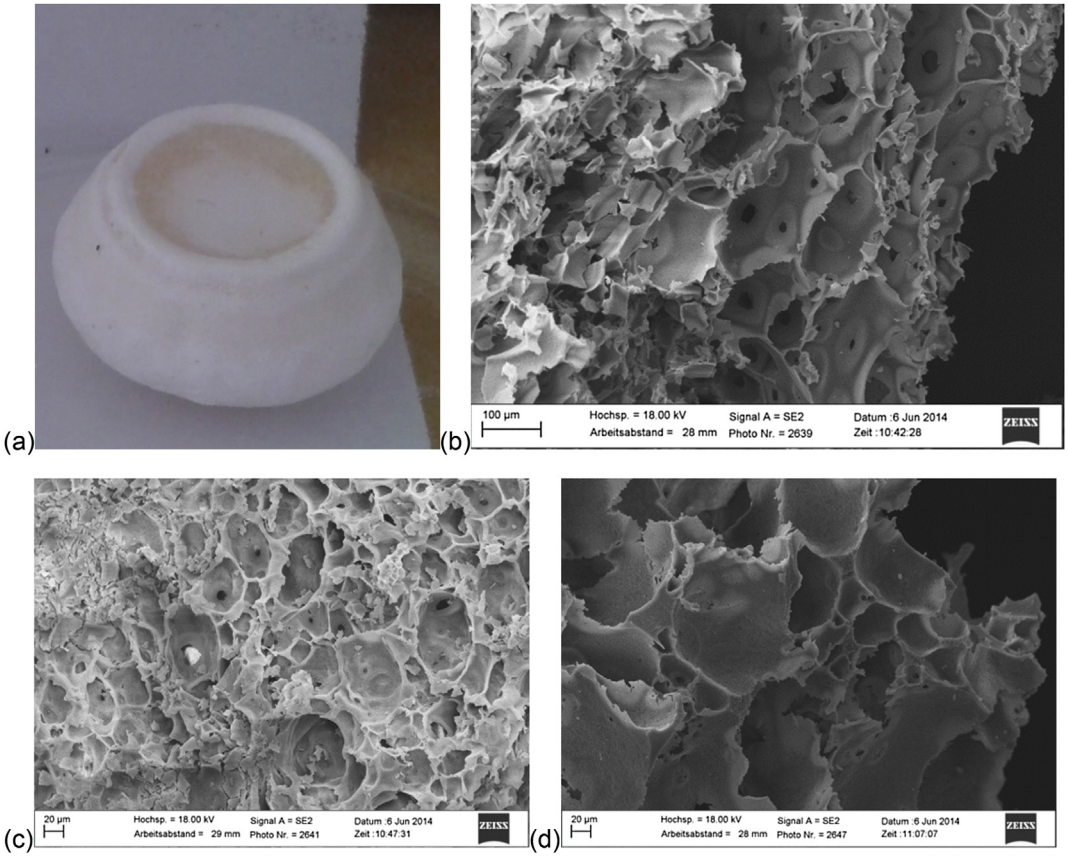

Fig. 4. (a) Bulk poly(NIPAM)HIPE (17 mol% MBA). Scanning electron microscopic images of poly(NIPAM)HIPEs with (b) 9 mol%, (c) 13 mol% and (d) 17 mol% *N,N′*-methylenebisacrylamide.

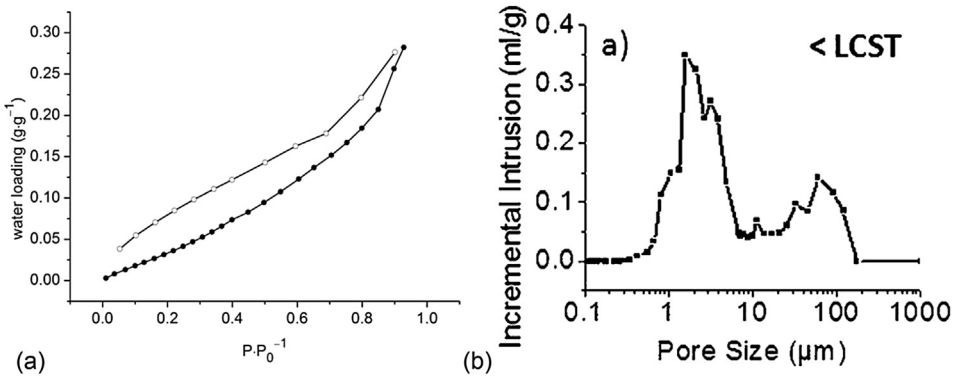

Fig. 5. (a) Water sorption isotherms of native poly(NIPAM)HIPE (17 mol% MBA) (degassing conditions: 3 h, 393 K). Adsorption is depicted with filled, desorption with empty symbols. (b) Pore size distribution curve of poly(NIPAM)HIPE (1% MBA cross-linking), from mercury intrusion measurements, adapted from Ref. [59].

bodies. Such changes to unsymmetrical morphologies upon polyHIPE drying are also apparent in the literature from photographs presented in Refs. [59,65,67].

The composites behave very similar in their swelling to pure NIPAM HIPE, e.g., in liquid water they absorb water under significant volume increase. For crosslinked alginate polyHIPE a water uptake of 8000% w/w was reported [65]. Upon drying the composites shrink again. Yet, in agreement with the literature [59,65] the swelling and shrinking is neither fully reversible in terms of the material structure and mechanical parameters nor does it occur under full retention of the original shape.

3.2.1. MIL-100(Fe)@NIPAM

MIL-100(Fe) embedded into poly(NIPAM)HIPE shows residual HIPE macropores with reduced void diameters in the scanning electron microscopic image (Fig. 6b). Octahedral MIL-100(Fe) particles with an average size of 2–5 µm are apparent, which adhere on the HIPE surface.

Powder X-ray diffraction patterns evidence the presence of crystalline MIL-100(Fe) in MIL-100(Fe)@NIPAM (Fig. 7a). Increasing the weight percentages of MIL leads to sharper reflections in the PXRD. Infrared spectra are a superposition of the individual spectra of both components (Fig. 7b).

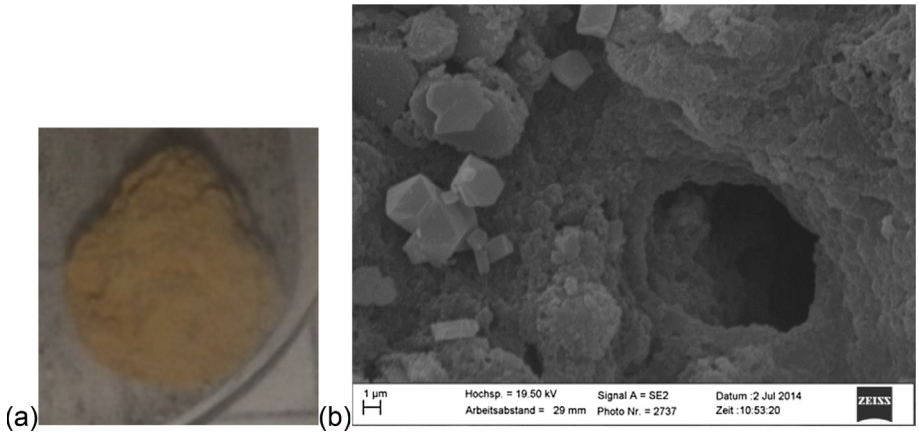

Fig. 6. (a) MIL-100(Fe)@NIPAM (78 wt% MIL). (b) Scanning electron microscopic images of MIL-100(Fe)@NIPAM (37 wt% MIL).

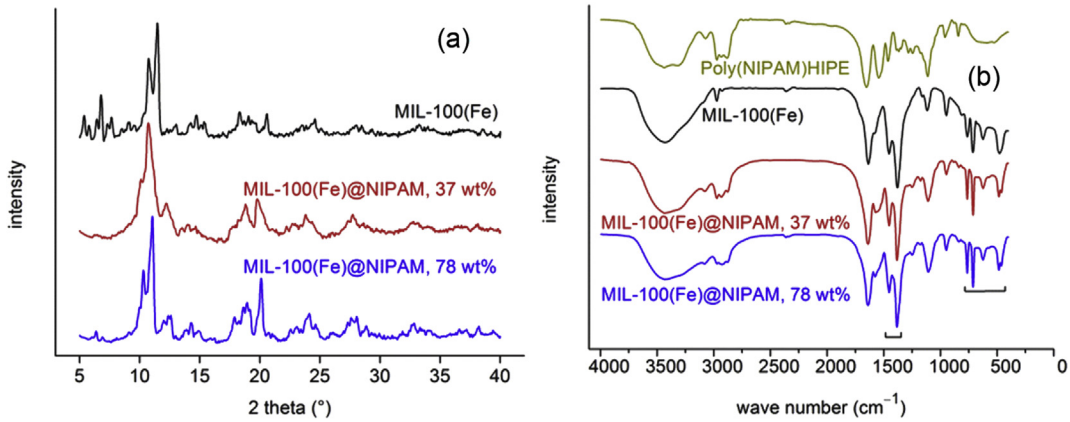

Fig. 7. (a) PXRD patterns of bulk MIL-100(Fe) and MIL-100(Fe)@NIPAM. (b) IR-spectra (KBr) of bulk poly(NIPAM)HIPE (17 mol% MBA), bulk MIL-100(Fe) and MIL-100(Fe)@NIPAM. Square brackets highlight the characteristic, asymmetric valence $\nu(R{-}CO_2)$, deformation $\delta(R{-}CO_2)-$ and $\nu(Fe{-}O)$ bands of MIL-100(Fe) in the composite material.

Fig. 8a presents the nitrogen sorption isotherms of poly(NIPAM) HIPE and the MIL-100(Fe)@NIPAM composites. Embedding of MIL-100(Fe) leads to an enhanced nitrogen uptake compared to the bulk HIPE, but less so than could be expected from their weight percent. Accessible micropores are evidenced in the composites through the corresponding pore size distribution curves (Fig. 8b).

BET surface area and total pore volume of native poly(NIPAM) HIPE with 20 $m^2\ g^{-1}$ and 0.03 $cm^3\ g^{-1}$ are increased in MIL-100(Fe) @NIPAMs with 230 $m^2\ g^{-1}$/0.12 $cm^3\ g^{-1}$ (37 wt% MIL) and 300 $m^2\ g^{-1}$/0.16 $cm^3\ g^{-1}$ (78 wt% MIL) (Table 1). Based on the weight percentages of MIL in MIL@NIPAM, the BET surface areas can be estimated according to formula d in Table 1. The expected values of 800 and 1650 $m^2\ g^{-1}$ for 37 and 78 wt% MIL containing composites indicate a high degree of MIL pore blocking effects. Consequently, water sorption isotherms show only a slight enhancement of water uptakes (Fig. 8c). The characteristic S-shaped water uptake between $0.35 < P \cdot P_0^{-1} < 0.4$ stems from the MIL part of the composite [39].

Because of time constraints – it takes about 2 days for a full water ad/desorption cycle to thermodynamic equilibrium – we have only measured one cycle here for each sample. The high water vapor ad/desorption cycle stability of MIL-100(Fe), MIL-100(Cr) and MIL-101(Cr) has been investigated and verified before [33,38,39]. Four cycles of loading from and release of polystyrene colloids in aqueous solution via porous NIPAM have been reported in Ref. [59]. Reloadings showed up to 90% of the initial loading. Repeated polystyrene loading and release could be achieved without apparent degradation of porous NIPAM.

3.2.2. MIL-100(Cr)@NIPAM

Powder X-ray diffraction patterns of MIL-100(Cr)@NIPAMs indicate the unchanged, crystalline phase of pure MIL-100(Cr) (Fig. 9a). Infrared spectra arise from the contribution of both components (Fig. 9b).

The nitrogen sorption isotherm (Fig. 10a) of both MIL-100(Cr) @NIPAMs composites show only a slightly increased gas uptake compared to pure poly(NIPAM)HIPE. The MIL-100(Cr)@NIPAMs are isotherms with a type II shape, which reflects the macroporous behavior of the HIPE. The hystereses between ad- and desorption isotherms refer to the presence of incorporated MIL mesopores. Pore size distribution curves of MIL-100(Cr)@NIPAMs document the existence of some mesopores and micropores of very poor resolution between 12 and 18 Å (Fig. 10b).

Hence, BET surface areas and total pore volumes of pure poly(-NIPAM)HIPE (20 $m^2\ g^{-1}$/0.03 $cm^3\ g^{-1}$) are only slightly enhanced in both composites (90 $m^2\ g^{-1}$/0.14 $cm^3\ g^{-1}$ for 49 wt%; 150 $m^2\ g^{-1}$/ 0.17 $cm^3\ g^{-1}$ for 58 wt%, Table 1). This is far below the estimated values of 680 $m^2\ g^{-1}$ (49 wt%) and 800 $m^2\ g^{-1}$ (58 wt%), presumably due to sizeable pore blocking, for example, by polymerization in the pore mouths. Thus, water sorption isotherms of MIL-100(Cr) @NIPAMs show little deviation from the curves for native HIPE (Fig. 10c).

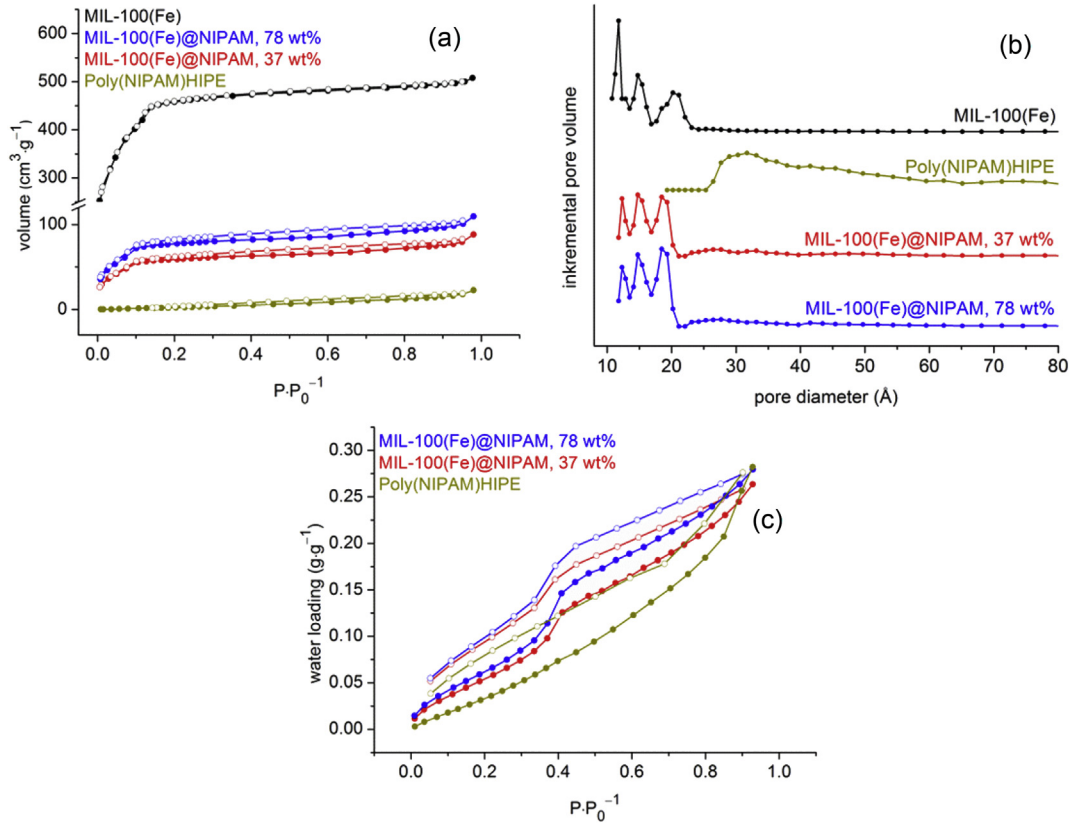

Fig. 8. (a) N_2-sorption isotherms and (b) pore size distribution curves of MIL-100(Fe)@NIPAM, bulk MIL-100(Fe) and bulk poly(NIPAM)HIPE (17 mol% MBA) (degassing conditions: 3 h, 393 K). (c) Water sorption isotherms of MIL-100(Fe)@NIPAM and bulk poly(NIPAM)HIPE (17 mol% MBA) (degassing conditions: 3 h, 393 K). Adsorption is depicted with filled, desorption with empty symbols.

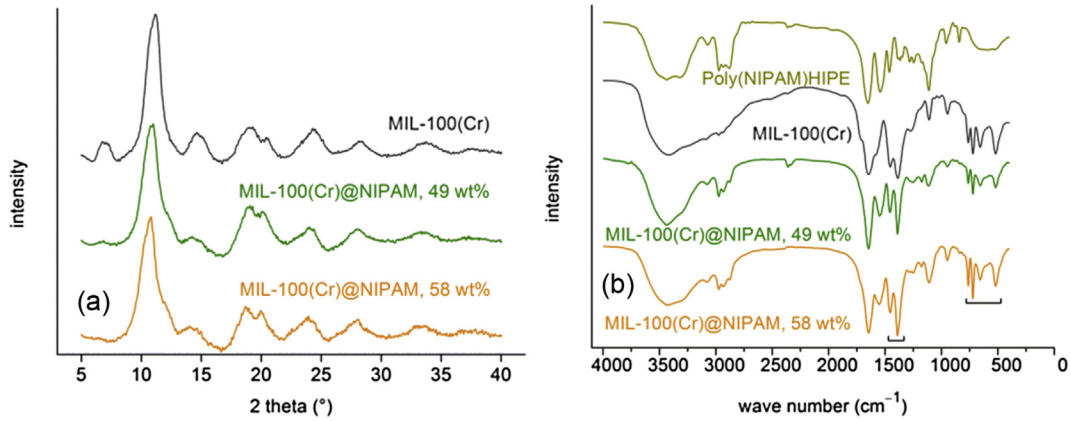

Fig. 9. (a) PXRD patterns of native MIL-100(Cr) and MIL-100(Cr)@NIPAM. (b) IR-spectra (KBr) of native MIL-100(Cr), native poly(NIPAM)HIPE (17 mol% MBA) and MIL-100(Cr)@NIPAM. Square brackets highlight the characteristic $\nu(R{-}CO_2)$ and $\nu(Cr{-}O)$ and deformation vibration $\delta(R{-}CO_2)$ bands of MIL-100(Cr) in the composite material.

3.2.3. *MIL-101(Cr)@NIPAM*

The scanning electron microscopic image of MIL-101(Cr)@NIPAM (92 wt%) visualized residual, macroporous HIPE pores with reduced void sizes compared to pure HIPE (Fig. 11b). MIL-101(Cr) particles of octahedral morphology with sizes of 0.3–0.5 μm stick onto the surface of the NIPAM-HIPE.

As seen before, retention of the crystalline MIL-101(Cr) phase in the composites is proven by powder X-ray diffraction patterns (Fig. 12a) and in the IR spectra the MIL-101 bands increase in intensity with percentage (Fig. 12b).

Different than seen before for the MIL-100 composites nitrogen sorption analyses of MIL-101(Cr)@NIPAM reveal a significant increase of gas uptake compared to native NIPAM-HIPE (Fig. 13a). All composite materials show microporous behavior due to the type I shaped sorption isotherms. Furthermore, these micropores can be evidenced by pore size distribution curves in Fig. 13b. Small hysteresis loops indicate the presence of MIL mesopores. Experimental surface areas of MIL-101(Cr)@NIPAM with 720 $m^2\ g^{-1}$ (46 wt%), 960 $m^2\ g^{-1}$ (71 wt%) and 980 $m^2\ g^{-1}$ (92 wt%) are also higher than for the MIL-100@NIPAM composites (Table 1). Thus,

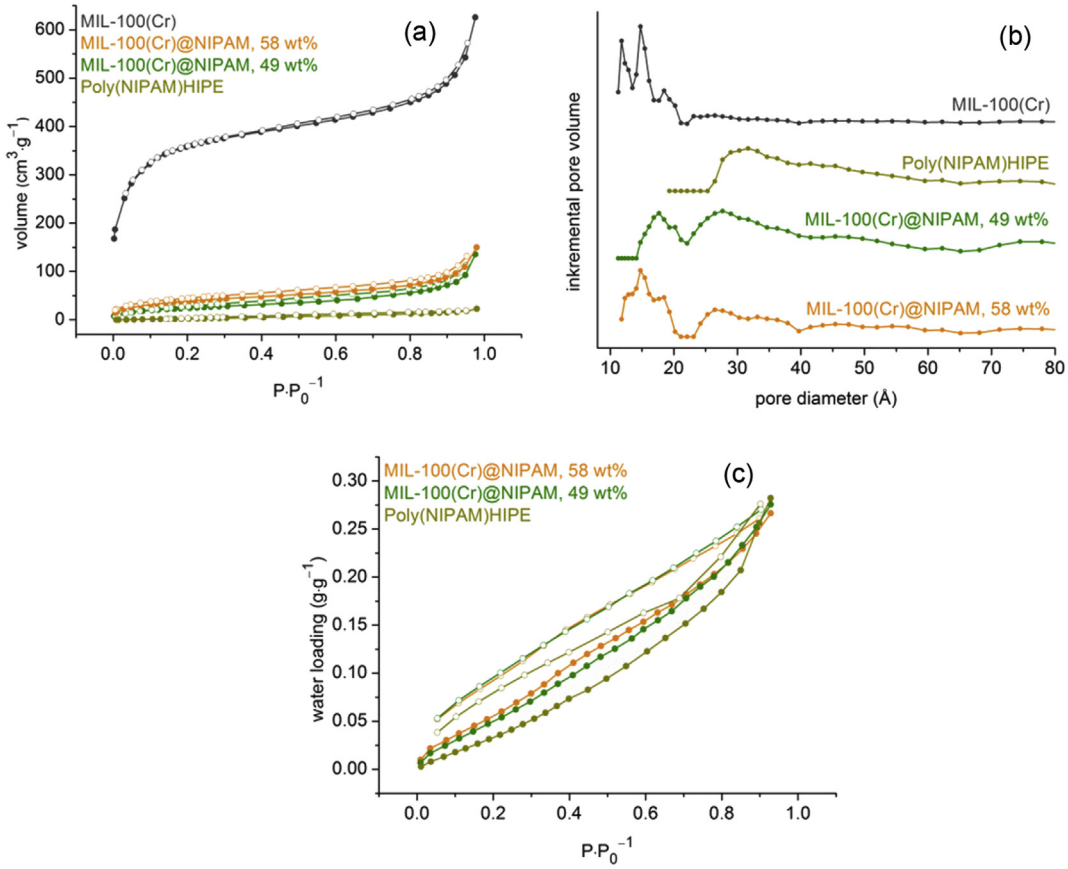

Fig. 10. (a) N_2-sorption isotherms and (b) pore size distribution curves of MIL-100(Cr)@NIPAM, native MIL-100(Cr) and native poly(NIPAM)HIPE (17 mol% MBA) (degassing conditions: 3 h, 393 K). (c) Water sorption isotherms of MIL-100(Cr)@NIPAM and native poly(NIPAM)HIPE (17 mol% MBA) (degassing conditions: 3 h, 393 K). Adsorption is depicted with filled, desorption with empty symbols.

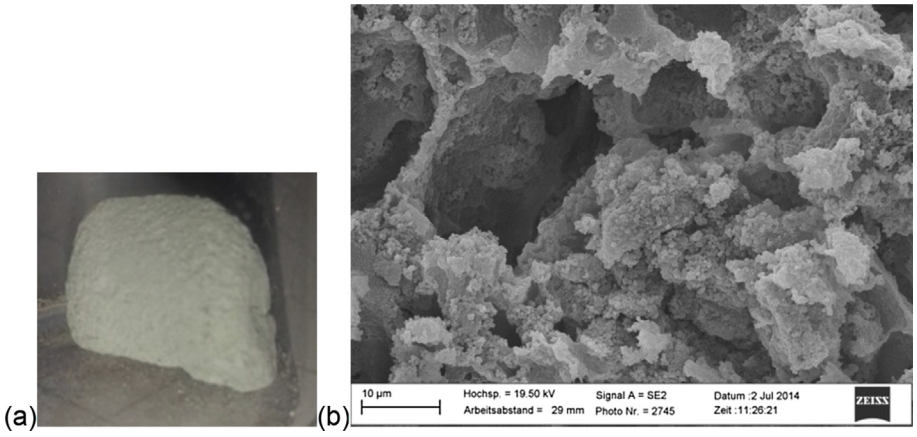

Fig. 11. (a) MIL-101(Cr)@NIPAM (92 wt% MIL). (b) Scanning electron microscopic images of MIL-101(Cr)@NIPAM (46 wt% MIL).

the water sorption isotherms of the composites show more satisfying results in comparison to MIL-100@NIPAMs, due to higher water vapor uptakes compared to pure HIPE over the entire pressure range (Fig. 13c). The stepwise and S-shaped water vapor sorption isotherms of the composites are characteristic of MIL-101(Cr) [24,33].

Nitrogen sorption isotherms, BET surface areas and pore size distribution curves show that embedding of MIL-101(Cr) leads to higher porous and therefore more efficient composites compared to MIL-100@NIPAMs. Experimental BET surface areas of MIL-101(Cr)@NIPAM are closer to the expected surface areas in comparison to both MIL-100@NIPAMs (Table 1). The free and accessible micropores in the MIL-101 composites lead to relatively high water vapor uptakes.

The larger BET surface areas of MIL-101(Cr) compared to MIL-100 composites, can be explained by a higher degree of pore blocking n the latter composites. Despite pre-polymerization poly(NIPAM)HIPE oligomers can more easily diffuse and thereby

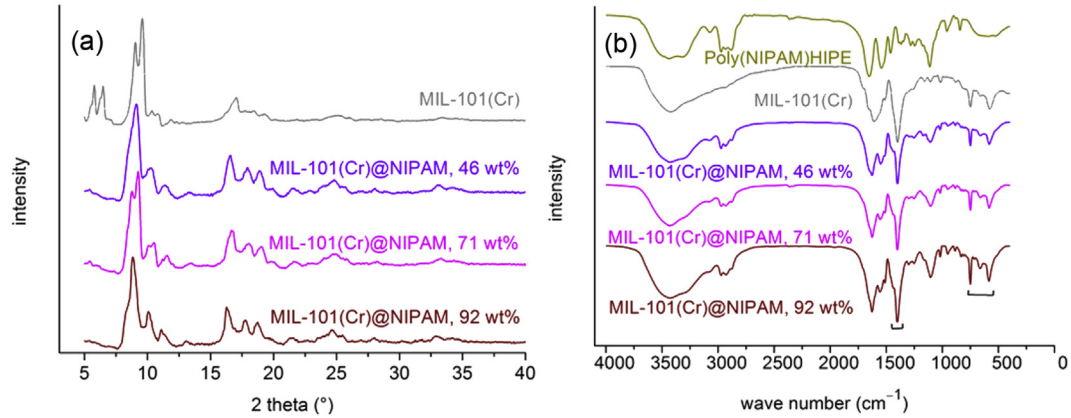

Fig. 12. (a) PXRD patterns of native MIL-101(Cr) and MIL-101(Fe)@NIPAM. (b) IR-spectra (KBr) of native MIL-101(Cr), native poly(NIPAM)HIPE (17 mol% MBA) and MIL-101(Cr)@NIPAM. Square brackets highlight the characteristic ν(R–CO_2) and ν(Cr–O) and deformation vibration δ(R–CO_2) bands of MIL-101(Cr) in the composite material.

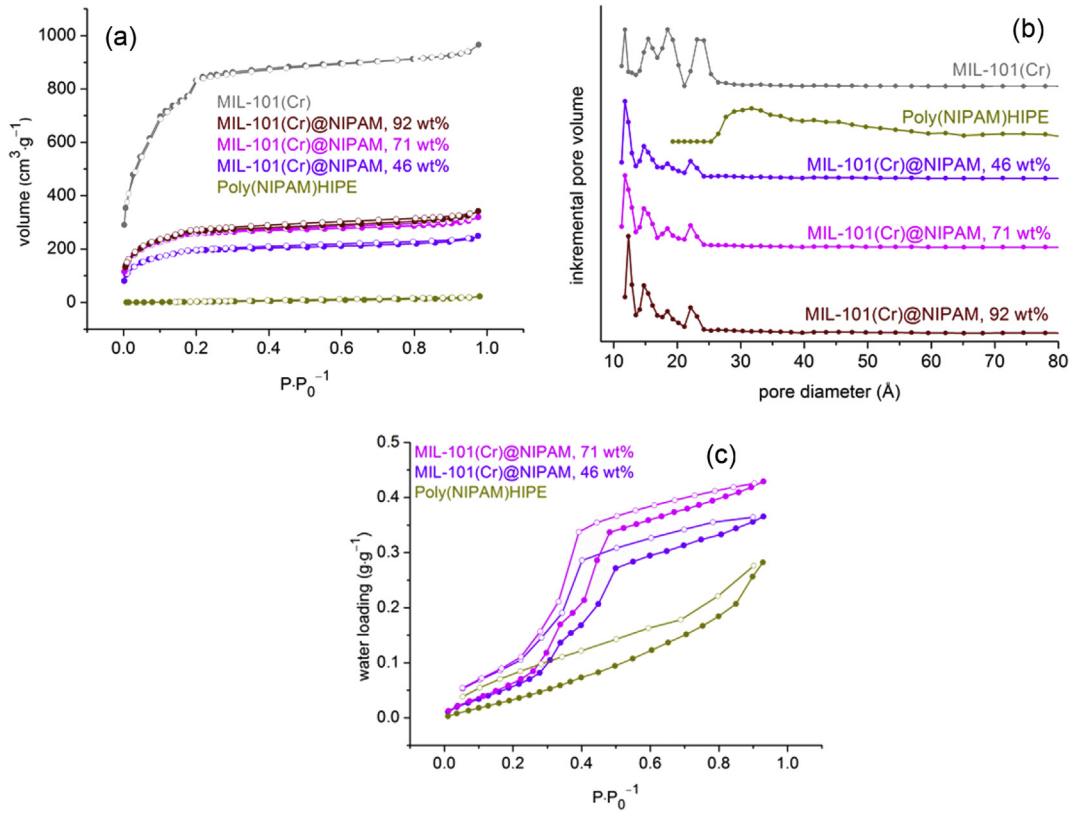

Fig. 13. (a) N_2-sorption isotherms and (b) pore size distribution curves of MIL-101(Cr)@NIPAM, native MIL-101(Cr) and native poly(NIPAM)HIPE (17 mol% MBA) (degassing conditions: 3 h, 393 K). (c) Water sorption isotherms of MIL-101(Cr)@NIPAM and native poly(NIPAM)HIPE (17 mol% MBA) (degassing conditions: 3 h, 393 K). Adsorption is depicted with filled, desorption with empty symbols.

block the smaller MIL-100 pores through filling of at least the pore mouths through stronger capillary condensation forces. The same phenomenon was observed for the MIL@R,F-xerogel composites [42].

Among both MIL-100@NIPAM composites, surface areas of MIL-100(Fe)@NIPAMs are closer to the expected BETs. Pore diameters of pure MIL-100(Fe) and MIL-100(Cr) are theoretically of the same size (25 and 29 Å), but BET surface areas show that pure MIL-100(Fe) (2140 m^2 g^{-1}) is much more porous than pure MIL-100(Cr) (1370 m^2 g^{-1}). The less porous MIL-100(Cr), incorporated in poly(NIPAM)HIPE, probably also shows pronounced pore blocking effects through higher capillary condensation forces. In other words: Smaller pores (or materials with lower inner surfaces) are more difficult to protect than larger pores (or materials with higher inner surfaces) (Scheme 2).

When we compare our results to the literature, syntheses of MOF composites with organic polymers is often accompanied with partial pore blocking. Other MOF composites show similar differences between experimental and estimated inner surface areas. HKUST-1, which was embedded in porous carbon monoliths, reaches only 40% of the estimated BET surface areas [68]. UiO-66@polyurethane or HKUST@HIPE achieve approximately 60% of

MIL-100(Cr)	MIL-100(Fe)	MIL-101(Cr)
BET = 1370 $m^2 \cdot g^{-1}$	2140 $m^2 \cdot g^{-1}$	2860 $m^2 \cdot g^{-1}$

higher BET surface areas/porosities
less capillary condensation forces
easier protection for composite syntheses

Scheme 2. Sequence of MIL pore protection for composite syntheses.

the estimated values [69,70]. These values are comparable to our MIL@NIPAM compounds.

The first report of a MOF-polymer composite was reported in 2008 with the *in situ* growth of HKUST-1 (Cu-BTC) in the voids of a pre-formed monolithic, macroporous polyHIPE, from 4-vinylbenzyl chloride and divinylbenzene [69]. An initial hydrophilization step of the polyHIPE by introduction of hydroxyl groups was necessary to obtain a homogeneous distribution of embedded MOF crystals. The HKUST-1@polyHIPE composite was synthesized by soaking the pure polyHIPE with MOF precursor solutions, followed by solvothermal treatment. The MOF loading depended on the number of impregnation steps with 62.3 wt% of Cu-BTC loading achieved after the third impregnation step with a maximum total surface area of 570 $m^2\ g^{-1}$ [69]. Similar HKUST-1 was grown *in situ* into pre-formed, macroporous, mm-sized PAM-HIPE beads (PAM = polyacrylamide), which were prepared using an emulsion-templated oil/water/oil (o/w/o) sedimentation polymerization technique [71]. The ratio of HKUST:PAM could be finely adjusted by changing the concentration of the HKUST precursors in the solution leading to different HKUST-1@PAM composites with a maximum Cu-BTC loading of 62 wt% and a BET surface area of 654 $m^2\ g^{-1}$ (BET of pure HKUST-1: 1075 $m^2\ g^{-1}$). A problem was that pre-swelling of the native PAM-HIPE beads in a solvent (without MOF precursors), prior to the MOF formation exclusively led to crystal growth on the external surface of the beads through prevention of diffusion into the bead interior [71].

The water adsorption value can also be related to the surface area measured in the MIL@NIPAM composite (last column in Table 1). The following trends became apparent: For most MIL@NIPAM composites the surface-based water adsorption is higher than for the MIL alone. This is especially so for MIL-100(M)s and shows the influence of the NIPAM matrix with its high surface area-based water adsorption value. Still, the MIL-100(Cr) composite has a significantly higher surface area-based water adsorption value than the MIL-100(Fe) composite. This is explained by the hierarchical contribution of the NIPAM matrix which adds significantly with diameters >20 Å for the chromium and less for the iron material according to the pore diameter distribution plots in Fig. 7 d and b. For the MIL-101(Cr) composite and bulk MIL-101(Cr) the surface area-based water uptake values of 0.44–0.5 × 10^{-3} g m^{-2} are very similar and reflect the dominance of MIL-101 in the composite material.

4. Conclusion

Pure poly(NIPAM)HIPE was obtained by an o/w emulsion using NIPAM as main monomer and MBA as cross-linker. Different mol% of cross-linkers were introduced into the porous polymers. It has been shown that only the highest amount of MBA with 17 mol% provided monolithic bodies in spite of strong shrinking effects (Scheme 3). Nevertheless, scanning electron microscopic images reveal the typical morphology with voids in μm range. Water sorption measurements have proven the rather hydrophobic nature of this pure HIPE.

Pre-polymerization of the HIPE emulsions before adding the MOF powders has turned out to be an indispensable step in synthesizing highly porous composites. Various amounts of MIL-100(Fe,Cr) and MIL-101(Cr) powders were added to the highly pre-polymerized HIPE emulsion. Unfortunately, addition of MOF powders did not avoid or minimize the expected shrinking effects of the composites, also seen for pure poly(NIPAM)HIPE. The direct route yielded composites with a maximum MOF loading of 92 wt% for MIL-101(Cr)@NIPAM, but deformation and shrinking was apparent in all MIL@NIPAM composites (Scheme 3).

The presence of MIL crystals in NIPAM composites was proven by powder patterns, infrared spectra and SEM images. Yet, nitrogen sorption studies revealed that pore blocking effects of the MIL pores by HIPE monomers occurred to a large extent, especially for both MIL-100@NIPAM composites.

Sorption analyses have shown that the experimental BET surface areas of MIL-100@NIPAM are below the estimated surface areas, based on the MOF weight percentages in the composites due to large pore blocking effects of the MIL-100 pores and windows by NIPAM and MBA monomers. MIL-100(Fe)@NIPAMs show more accessible and free MIL micropores compared to MIL-100(Cr)@NIPAMs, based on BET and pore size distribution analyses. Due to the large pore blocking effects, water sorption measurements of MIL-100@NIPAMs reveal only slightly enhanced water uptakes over the entire pressure range in comparison to the pure HIPE.

In contrast, experimental surface areas of MIL-101(Cr)@NIPAMs are closer to the estimated BETs, when compared to MIL-100(*M*)@NIPAM. Pore blocking effects seem to be less pronounced, possibly due to lower capillary condensation forces because of the larger MIL-101 pores and windows. Water sorption isotherms of MIL-101(Cr)@NIPAM show increased water vapor uptakes compared to MIL-100@NIPAMs.

Scheme 3. Synthetic route to synthesize MIL@poly(NIPAM)HIPE (MIL-100(Fe,Cr), MIL-101(Cr)). Only MIL-100(Fe)@NIPAM and MIL-101(Cr)@NIPAM composites are shown.

Acknowledgements

We thank Mr. Steffen Köhler for obtaining the SEM images. The work was funded in part by BMBF project OptiMat 03SF0492C and in part by DAAD PPP project China 2j ab 14.

Appendix A. Supplementary data

Supplementary data related to this article can be found at http://dx.doi.org/10.1016/j.micromeso.2015.09.008.

References

[1] (a) S.R. Batten, N.R. Champness, X.-M. Chen, J. Garcia-Martinez, S. Kitagawa, L. Öhrström, M. O'Keeffe, M.P. Suh, J. Reedijk, Cryst. Eng. Comm. 14 (2012) 3001–3004;
(b) S.R. Batten, N.R. Champness, X.-M. Chen, J. Garcia-Martinez, S. Kitagawa, L. Öhrström, M. O'Keeffe, M.P. Suh, J. Reedijk, Pure Appl. Chem. 85 (2013) 1715–1724.
[2] J.R. Long, O.M. Yaghi, Chem. Soc. Rev. 38 (2009) 1213–1214.
[3] S. Kitagawa, S. Natarajan, Eur. J. Inorg. Chem. 24 (2010) 3685.
[4] C. Serre, S. Kitagawa, P.D.C. Dietzel, Micropor. Mesopor. Mater. 157 (2012) 1–2.
[5] M. Yoon, R. Srirambalaji, K. Kim, Chem. Rev. 112 (2012) 1196–1231.
[6] D. Farrusseng, S. Aguado, C. Pinel, Angew. Chem. Int. Ed. 48 (2009) 7502–7513.
[7] J. Lee, O.K. Farha, J. Roberts, K.A. Scheidt, S.T. Nguyen, J.T. Hupp, Chem. Soc. Rev. 38 (2009) 1450–1459.
[8] A. Herbst, A. Khutia, C. Janiak, Inorg. Chem. 53 (2014) 7319–7333.
[9] F.X. Llabrés i Xamena, F.G. Cirujano, A. Corma, Micropor. Mesopor. Mater. 157 (2012) 112–117.
[10] R.B. Getman, Y.-S. Bae, C.E. Wilmer, R.Q. Snurr, Chem. Rev. 112 (2012) 703–723.
[11] Z. Chen, S. Xiang, H.D. Arman, P. Li, S. Tidrow, D. Zhao, B. Chen, Eur. J. Inorg. Chem. 24 (2010) 3745–3749.
[12] F. Ma, S. Liu, D. Liang, G. Ren, C. Zhang, F. Wei, Z. Su, Eur. J. Inorg. Chem. 24 (2010) 3756–3761.
[13] L. Wu, M. Xue, S.-L. Qiu, G. Chaplais, A. Simon-Masseron, J. Patarin, Micropor. Mesopor. Mater. 157 (2012) 75–81.
[14] Z. Zhang, Y. Zhao, Q. Gong, Z. Li, J. Li, Chem. Commun. 49 (2013) 653–661.
[15] J.-R. Li, Y. Ma, M.C. McCarthy, J. Sculley, J. Yu, H.-K. Jeong, P.B. Balbuena, H.-C. Zhou, Coord. Chem. Rev. 155 (2011) 1791–1823.
[16] J.-R. Li, J. Sculley, H.-C. Zhou, Chem. Rev. 112 (2012) 869–932.
[17] Z.R. Herm, R. Krishna, J.R. Long, Micropor. Mesopor. Mater. 157 (2012) 94–100.
[18] M.G. Plaza, A.F.P. Ferreira, J.C. Santos, A.M. Ribeiro, U. Müller, N. Trukhan, J.M. Loureiro, A.E. Rodrigues, Micropor. Mesopor. Mater. 157 (2012) 101–111.
[19] C. Janiak, Dalton Trans. 14 (2003) 2781–2804.
[20] C. Janiak, J.K. Vieth, New J. Chem. 34 (2010) 2366–2388.
[21] H.B. Tanh Jeazet, C. Staudt, C. Janiak, Dalton Trans. 41 (2012) 14003–14027.
[22] G. Férey, Chem. Soc. Rev. 37 (2008) 191–214.
[23] M. Gaab, N. Trukhan, S. Maurer, R. Gummaraju, U. Müller, Micropor. Mesopor. Mater. 157 (2012) 131–136.
[24] S.K. Henninger, F. Jeremias, H. Kummer, C. Janiak, Eur. J. Inorg. Chem. (2012) 2625–2634.
[25] F. Jeremias, D. Fröhlich, C. Janiak, S.K. Henninger, New J. Chem. 38 (2014) 1846–1852.
[26] C. Janiak, S.K. Henninger, Chimia 67 (2013) 419–424.
[27] (a) Y.I. Aristov, Int. J. Refrig. 32 (2009) 675–686;
(b) B.B. Saha, A. Chakarborty, S. Koyama, Y.I. Aristov, Int. J. Heat. Mass Transf. 52 (2009) 516–524;
(c) R.E. Critoph, Z. Tamainot-Telto, S.J. Metcalf, Int. J. Refrig. 32 (2009) 1212–1229;
(d) J.V. Veselovskaya, R.E. Critoph, R.N. Thorpe, S. Metcalf, M.M. Tokarev, Y.I. Aristov, Appl. Therm. Eng. 30 (2010) 1188–1192.
[28] K. Habib, B.B. Saha, A. Chakraborty, S.T. Oh, S. Koyama, Appl. Therm. Eng. 50 (2013) 1582–1589.
[29] A.A. Askalany, M. Salem, I.M. Ismael, A.H.H. Ali, M.G. Morsy, B.B. Saha, Renew. Sust. Energy Rev. 19 (2013) 565–572.
[30] D. Fröhlich, S.K. Henninger, C. Janiak, Dalton Trans. 43 (2014) 15300–15304.
[31] C. Li, J. Zhou, Y. Cao, J. Zhong, Y. Liu, C. Kang, Y. Tan, Appl. Energy 117 (2014) 149–156.
[32] G. Férey, C. Mellot-Draznieks, C. Serre, F. Millange, J. Dutour, S. Surblé, I. Margiolaki, Science 309 (2005) 2040–2042.
[33] J. Ehrenmann, S.K. Henninger, C. Janiak, Eur. J. Inorg. Chem. 4 (2011) 471–474.
[34] K. Brandenburg, Diamond (Version 3.2), Crystal and Molecular Structure Visualization, Crystal Impact, K. Brandenburg & H. Putz Gbr, Bonn (Germany), 2009.
[35] G. Férey, C. Serre, C. Mellot-Draznieks, F. Millange, S. Surble, J. Dutour, I. Margiolaki, Angew. Chem. Int. Ed. 43 (2004) 6296–6301.
[36] P. Horcajada, S. Surble, C. Serre, D.-Y. Hong, Y.-K. Seo, J.-S. Chang, J.-M. Grenèche, I. Margiolaki, G. Férey, Chem. Commun. 27 (2007) 2820–2822.
[37] C. Volkringer, D. Popov, T. Loiseau, G. Férey, M. Burghammer, C. Riekel, M. Haouas, F. Taulelle, Chem. Mater. 21 (2009) 5695–5697.
[38] G. Akiyama, R. Matsuda, S. Kitagawa, Chem. Lett. 39 (2010) 360–361.
[39] F. Jeremias, A. Khutia, S.K. Henninger, C. Janiak, J. Mater. Chem. 22 (2012) 10148–10151.
[40] M. Wickenheisser, C. Janiak, Micropor. Mesopor. Mater. 204 (2015) 242–250.
[41] V. Finsy, L. Ma, L. Alaerts, D.E. De Vos, G.V. Baron, J.F.M. Denayer, Micropor. Mesopor. Mater. 120 (2009) 221–227.
[42] M. Wickenheisser, A. Herbst, R. Tannert, B. Milow, C. Janiak, Micropor. Mesopor. Mater. 215 (2015) 143–153.
[43] D. Bradshaw, A. Garai, J. Huo, Chem. Soc. Rev. 41 (2012) 2344–2381.
[44] O.-L. Zhu, Q. Xu, Chem. Soc. Rev. 43 (2014) 5468–5512.
[45] D. Barby, Z. Haq, Eur. Pat., 1982. EP 60138 A1 19820915.
[46] (a) S.D. Kimmins, N.R. Cameron, Adv. Funct. Mater. 21 (2011) 211–225;
(b) H. Zhang, A.I. Cooper, Soft Matter 1 (2005) 107–113.
[47] N. Cohen, M.S. Silverstein, Polymer 52 (2011) 282–287.
[48] S. Kovačič, K. Jeřabek, P. Krajnc, Macromol. Chem. Phys. 212 (2011) 2151–2158.
[49] P. Krajnc, N. Leber, D. Stefanec, S. Kontrec, A.J. Podgornik, Chromatogr. A 1065 (2005) 69–73.
[50] E.M. Christenson, W. Soofi, J.L. Holm, N.R. Cameron, A.G. Mikos, Biomacromolecules 8 (2007) 3806–3814.
[51] D. Štefanec, P. Krajnc, Polym. Int. 56 (2007) 1313–1319.
[52] O. Kulygin, M.S. Silverstein, Soft Matter 3 (2007) 1525–1529.
[53] L.D. Gelb, K.E. Gubbins, R. Radhakrsihan, M. Sliwinska-Bartowiak, Rep. Prog. Phys. 62 (1999) 1573–1659.
[54] N.A. Sedron, J.P.R.B. Walton, N. Quirke, Carbon 27 (1989) 853–861.
[55] A. Vishnyakov, P. Ravikovitch, A.V. Neimark, Langmuir 16 (2000) 2311–2320.
[56] J.W. Yoon, Y.-K. Seo, Y.K. Hwang, J.-S. Chang, H. Leclerc, S. Wuttke, P. Bazin, A. Vimont, M. Daturi, E. Bloch, P.L. Llewellyn, C. Serre, P. Horcajada, J.-M. Grenèche, A.E. Rodrigues, G. Férey, Angew. Chem. Int. Ed. 49 (2010) 5949–5952.
[57] A. Vimont, J.-M. Goupil, J.-C. Lavalley, M. Daturi, S. Surblé, C. Serre, F. Millange, G. Férey, N. Audebrand, J. Am. Chem. Soc. 128 (2006) 3218–3227.
[58] J. Yang, Q. Zhao, J. Li, J. Dong, Micropor. Mesopor. Mater. 130 (2010) 174–179.
[59] (a) N.C. Grant, A.I. Cooper, H. Zhang, Appl. Mater. Interfaces 2 (2010) 1400–1406;
(b) H. Zhang, A.I. Cooper, Adv. Mater. 19 (2007) 2439–2444.
[60] N. Brun, S. Ungureanu, H. Deleuze, R. Backov, Chem. Soc. Rev. 40 (2011) 771–788.
[61] N. Cameron, Polymer 46 (2005) 1439–1449.
[62] T. Hasegawa, S. Tatsuta, Y. Katsumoto, Anal. Bioanal. Chem. 398 (2010) 2203–2209.
[63] K.S.W. Sing, D.H. Everett, R.A.W. Haul, L. Moscou, R.A. Pierotti, J. Rouquerol, T. Siemieniewska, Pure Appl. Chem. 57 (1985) 603–619.
[64] E.-P. Ng, S. Mintova, Micropor. Mesopor. Mater. 114 (2008) 1–26.
[65] (a) S. Zhou, A. Bismarck, J.H.G. Steinke, J. Mater. Chem. B 1 (2013) 4736–4745;
(b) F. Audouin, A. Heise, Eur. Polym. J. 49 (2013) 1073–1079.
[66] N.D. Banker, K. Srinivasan, M. Prasad, Carbon 42 (2004) 117–127.
[67] M.G. Schwab, I. Senkovska, M. Rose, N. Klein, M. Koch, J. Pahnke, G. Jonschker, B. Schmitz, M. Hirscher, S. Kaskel, Soft Matter 5 (2009) 1055–1059.
[68] D. Qian, C. Lei, G.-P. Hao, W.-C. Li, A.-H. Lu, Appl. Mater. Interfaces 4 (2012) 6125–6132.
[69] M.L. Pinto, S. Dias, J. Pires, Appl. Mater. Interfaces 5 (2013) 2360.
[70] M.G. Schwab, I. Senkovska, M. Rose, M. Koch, J. Pähnke, G. Jonschker, S. Kaskel, Adv. Eng. Mater. 10 (2008) 1151–1155.
[71] L.D. O'Neill, H. Zhang, D. Bradshaw, J. Mater. Chem. 20 (2010) 5720–5726.